16th World Conference on Earthquake Engineering, 16WCEE 2017

Santiago Chile, January 9th to 13th 2017

Paper N° 3921

Registration Code: S-P1464297289

SELF-CENTERING, LOW-DAMAGE, PRECAST POST-TENSIONED COLUMNS FOR ACCELERATED BRIDGE CONSTRUCTION IN SEISMIC REGIONS

G. Guerrini(1), J.I. Restrepo(2), M.J. Schoettler(3)

(1) Post-Doctoral Researcher, Dept. of Civil Engineering and Architecture, University of Pavia, Italy – gabriele.guerrini@eucentre.it
(2) Professor, Dept. of Structural Engineering, University of California, San Diego – jrestrepo@ucsd.edu
(3) Research Engineer, Pacific Earthquake Engineering Research Center, University of California, Berkeley – schoettler@berkeley.edu

Abstract

An innovative bridge column technology for application in seismic regions has been developed at the University of California, San Diego, in collaboration with the Pacific Earthquake Engineering Research Center. The proposed technology combines a precast composite steel-concrete hollow-core column, with post-tensioning and supplemental energy dissipation. Seismic resilience is enhanced in the form of self-centering capability, facilitation of structural fuse repair, and minimization of damage to the main structural elements.

The precast hollow-core column consists of two concentric cylindrical steel shells, with concrete sandwiched in between. The shells act as permanent formwork, the outer one substituting the conventional reinforcing cage by flexure and shear resistance as well as acting as confining reinforcement, and the inner shell preventing concrete from imploding. These features are aimed at improving constructability and reducing on-site construction burdens, thus making the technology suitable for accelerated bridge construction.

Large inelastic rotations can be accommodated at the end joints with minimal structural damage: gaps are allowed to open in tension at these locations and to close upon load reversal. Post-tensioned longitudinal bars induce self-centering behavior in combination with gravity forces. Elastomeric pads, placed in series with the post-tensioning bars at their anchorages, protect them from yielding. Specifically designed steel devices across the joints provide energy dissipation by axial hysteresis. High-performance grout and headed reinforcement are used to prevent premature crushing of the mortar joints, required by construction tolerances.

This paper summarizes the results obtained from dynamic shake-table tests, as well as from numerical simulations carried out in OpenSees. The superior performance of the proposed technology is also compared to that of conventional reinforced-concrete columns.

Keywords: Precast bridge column; Hysteretic energy dissipation; Hybrid rocking; Post-tensioning; Self-centering.

1. Introduction

Current provisions for the seismic design of bridges in the United States allow columns to respond beyond the elastic limit and to be damaged under the design earthquake, provided that collapse is prevented [1][2]. Inelastic behavior is localized within flexural plastic-hinge regions at the bottom and/or top of the columns. These regions may experience some structural damage which may lead to temporary closure of the bridge to the public. However, the consequences could be critical if associated with the interruption of an important road path: obstruction of rescue and recovery operations, and economical losses related to business interruption and displacement of people and goods [3].

While the notion of structural damage is accepted in design, resilient communities expect bridges to survive a moderately strong earthquake with little or no disturbance to traffic: this implies that partial or total bridge closures are tolerated with uneasiness, particularly in heavily congested urban areas. As a consequence, research efforts have been prompted into advanced technologies that minimize structural damage, encompass self-centering properties [4][5][6][7][8][9][10][11][12][13], and reduce construction time and impacts [14][15]. Moreover, these innovative solutions need to be economically and practically viable when compared to existing technologies in order to facilitate their adoption by the construction industry [16].

This paper describes the main outcomes of an experimental and analytical work on a self-centering, post-tensioned, precast composite steel-concrete column, which is an enhancement to earlier research conducted by the authors [17][18][19]. The use of precast members, the replacement of traditional time-consuming reinforcing cages with steel pipes, and the adoption of lighter hollow cross-sections are aimed at improved constructability and reduced on-site burdens. In parallel, the combination of unbonded post-tensioned connections with specific energy dissipating devices ensure seismic resilience, in the form of self-centering behavior, facilitation of structural fuse repair, and minimization of damage to the main structural elements. As a consequence, traffic impacts, environmental disruptions, and life-cycle costs can be reduced.

2. System Description

The precast bridge column described in this paper consists of two concentric cylindrical steel shells (*dual-shell* technology) running for its entire height, with high-performance concrete cast in between (Fig. 1a). The outer shell acts as permanent formwork, and provides longitudinal and transverse reinforcement in composite action with the concrete. The inner shell provides permanent formwork too, reducing unnecessary weight and making the technology suitable for prefabrication and rapid erection. It also prevents concrete implosion under large compressive strains which may develop upon gap opening, and delays buckling of energy dissipating dowels which are embedded in the concrete.

Large inelastic rotations can be sustained at the column-footing and column-cap beam joints with minimal structural damage. These rotations are accommodated within the connections themselves (Fig. 1b): gaps are allowed to open in tension under severe lateral displacement demand, and to practically close at the end of the excitation. Self-centering/rocking capability is provided by gravity forces and unbounded, threaded post-tensioning (PT) bars, designed to remain elastic. The bolted PT bar anchorages at the bent cap and foundation allow for eventual bar replacement, should corrosion or other damage be a concern.

Energy dissipation takes place through axial yielding of internal dowels through the rocking interfaces [17][20], as shown in Fig. 1b, preventing the main structural members from experiencing significant damage. Under strong-intensity earthquake excitation only these devices may undergo multiple cycles within the inelastic range, with possible need of replacement, but the structure is expected to remain functional overall. Circumferential weld beads are provided on the internal surface of the outer shell, only near its ends, to enhance composite action in transferring tension between the internal dowels and the outer shell [17][21]. The resulting lateral force-displacement response shows flag-shaped loops as illustrated in Fig. 1c.

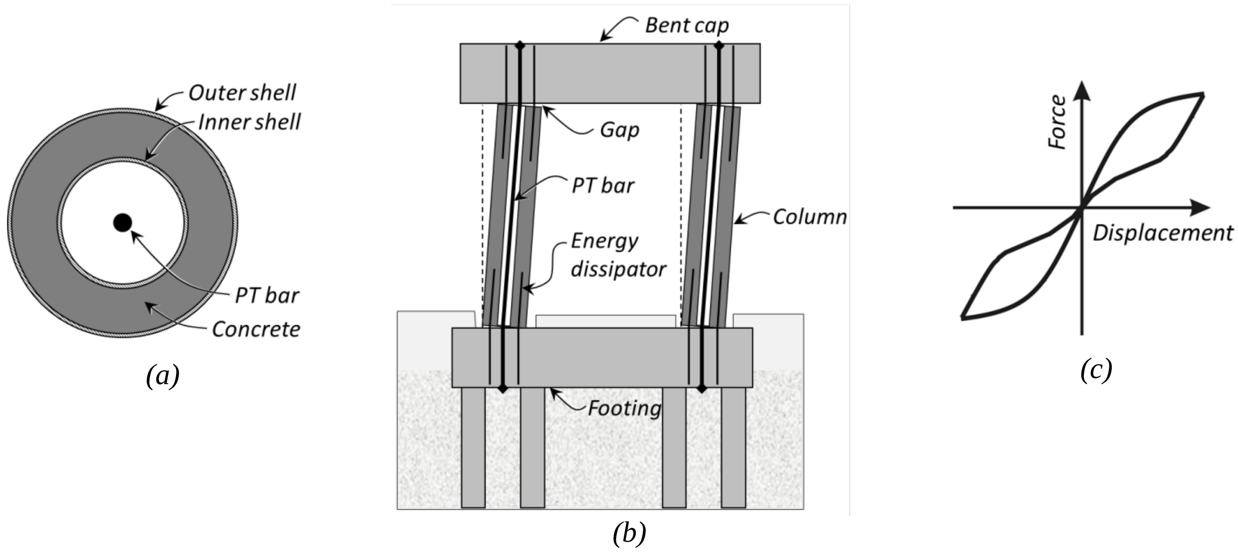

Fig. 1 – Schematic representation of the proposed technology: (a) column typical cross-section; (b) bent components and rocking kinematics; (c) flag-shaped hysteretic response.

3. Experimental Background

Restrepo et al. [17] conducted a quasi-static cyclic test on a dual-shell self-centering column (Unit HYB3) in cantilever configuration, at 1-to-2.4 scale. Self-centering behavior was induced by gravity forces and post-tensioning strands. Energy dissipation was provided by eight stainless-steel dowel bars crossing the column-footing interface. A hydraulic cement-based mineral-aggregate high strength, non-shrink grout was used for the mortar bed between the column and the footing.

The unit was subjected to lateral displacement cycles of increasing amplitude. The mortar bed started flaking off during cycles to 0.5% drift ratio, and started crushing at 0.75% drift ratio; damage was initiated by the stiff outer steel shell, transferring direct compression to the weaker mortar. Energy dissipating dowel fractures were observed after reaching a drift ratio of 6%. Self-centering capacity was prematurely lost during 3% drift ratio cycles, when residual drift ratios of the order of 1% were recorded; strength degradation was observed at this stage of the test as well. This behavior was caused by the degradation of the mortar layer, which led to an overall shortening of the unit: the consequent loss of post-tensioning force caused a reduction in the lateral strength, and in the magnitude of the recentering force (post-tensioning plus gravity) relatively to the overstrength of the energy dissipating dowels.

Guerrini et al. [18][19] tested another dual-shell column (Unit 1B) with similar dimensions, test layout, and loading protocol. However, post-tensioning threaded rods were used instead of strands: in fact, anchor wedges may cause strand fracture under cycling loading [22], and strand replacement could be a major issue compared to bar substitution in case of corrosion or other damage. Special care was dedicated to the mortar bed: a high-performance metallic-aggregate grout was used, and polypropylene fibers were added in the proportion of 0.035% by weight to increase the mortar toughness. The mortar was removed from below the outer steel shell, to avoid direct contact and premature initiation of crushing.

Improvements were observed in the performance under cyclic lateral loading compared to Restrepo et al. [17]. Mortar bed started crushing during 5%-drift-ratio cycles. Energy-dissipating dowels fractured after reaching a drift ratio of 7.5%. Self-centering behavior was maintained up to 5%-drift-ratio cycles, when stiffness degradation, but not strength degradation, became evident. Self-centering capability was significantly compromised during 7.5%-drift-ratio cycles.

4. Shake-Table Test

4.1 Test Specimen

A dual-shell column specimen was built at 1-to-3 scale at the Powell Structural Engineering Laboratories of the University of California, San Diego, and tested on the shake-table of the Pacific Earthquake Engineering Center (PEER) Laboratory at the University of California, Berkeley. It was loaded in a cantilever configuration, with fixed base and an inertial mass applied at the top, as shown in Fig. 2. The column had an overall diameter of 0.41 m (16 in.) and a height of 1.32 m (52 in.); the total cantilever span from the base to the center of mass was 2.44 m (96 in.). Column, footing, and loading stub were precast separately, and then connected through grouted dowels and a post-tensioning rod. Three inertial mass blocks were subsequently attached to the loading stub.

The column outer shell had a diameter D_O = 0.41 m (16 in.) and a thickness t_O = 6.4 mm (0.25 in.), that is D_O / t_O = 64. The inner shell had a diameter D_I = 0.25 m (10 in.) and a thickness t_I = 3.2 mm (0.125 in.), that is D_I / t_I = 80. Details are shown in Fig. 3. The shells were obtained by folding and welding plates made of Grade 50 A572 steel; in practice, the inner shell would be a corrugated drainage pipe [17]. High-performance, normal-weight concrete was used to cast column, footing, and load stub. The specified concrete compressive strength at 56 days was 62 MPa (9.0 ksi), the ones measured at 28 days, 56 days, and 101 days (day of test) were 60 MPa (8.7 ksi), 66 MPa (9.6 ksi) and 70 MPa (10.2 ksi), respectively.

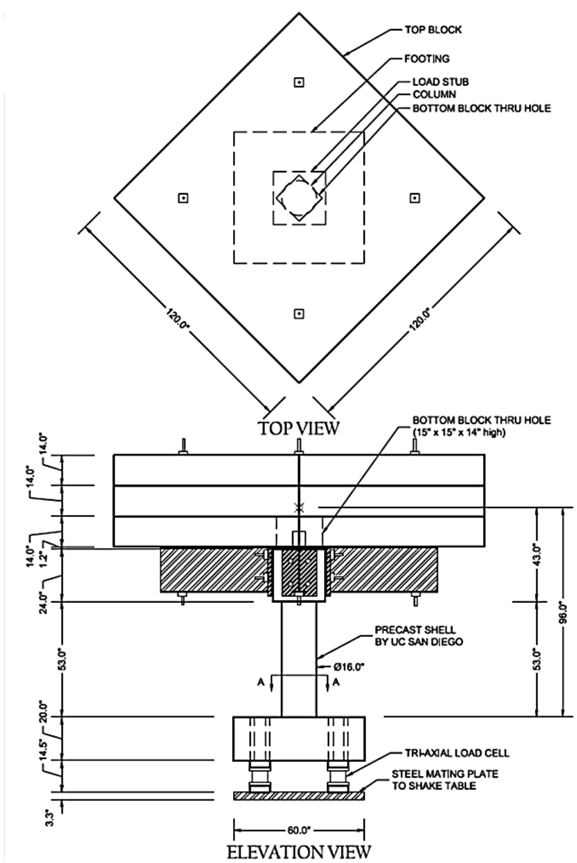

Fig. 2 – Test setup and dimensions.

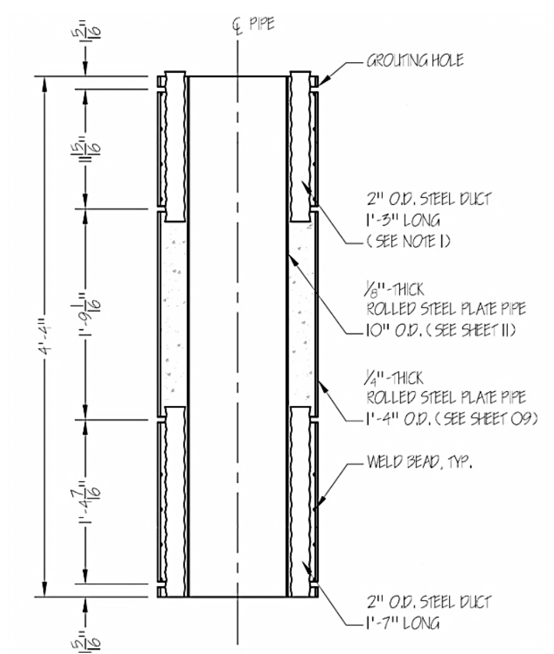

Fig. 3 – Column vertical section.

Eight 50.8-mm- (2-in.-) diameter, 0.48-m (19-in) long, corrugated steel ducts were embedded in the concrete for the installation of the internal energy-dissipating dowels at the column bottom (Fig. 3 and Fig. 4a). Eight similar ducts, 0.38-m (15-in.) long, were placed at the top for grouting the load-stub dowels (Fig. 3 and Fig. 5a). Four circumferential 9.5-mm (3/8-in.) weld beads on the internal surface of the outer shell provided tensile stress transfer between the dowels and the shell at each end.

A 19-mm (0.75-in.) thick mortar bed was cast between the column and the footing, to simulate compensation for expected in-situ construction tolerances. Upon rocking, large compressive strains may arise on the mortar; eventually, mortar crushing would cause loss of PT and loss of self-centering capacity. Thus, a high-performance mix was used, with the addition of polypropylene fibers in the proportion of 0.035% by weight to increase the mortar toughness. Moreover, the mortar was scraped from underneath the outer shell, to prevent the shell from causing premature crushing under direct compression transfer, a problem noted in earlier experiments [17]. Strengths of 104 MPa (15.1 ksi) and 120 MPa (17.5 ksi) were obtained at 28 and 73 days (day of test), respectively. Eight headed bars were embedded in the column and eight in the footing, with their heads matching at the interface (Fig. 4), to help the mortar transferring compression [22]. The upper joint between the column and the load stub, not critical because of the lower bending moment at this location, was realized with the same mortar but without headed bars. All interface surfaces were roughened to improve shear friction. Bond breaker was applied to the surface of the footing, to allow separation from the mortar bed and opening of the gap.

The unit was equipped with eight internal dowels at the column-footing joint, acting as internal energy dissipators (Fig. 4b). 316LN Grade 75 stainless steel #3 (9.5-mm-diameter) bars were used for this purpose, wrapped with duct tape for 152 mm (6 in.) across the interface to destroy the bond within this length. Material testing provided a yield stress of 862 MPa (125 ksi), peak strength of 986 MPa (143 ksi), and peak strain of 10%. The dowels were tied together with the footing cage and, after the column had been placed on the footing, they were grouted within the column ducts. Similarly, eight dowels were provided to connect the load stub to the column (Fig. 5a); however, A706 Grade 60 steel #4 (12.7-mm-diameter) reinforcing bars without duct-tape wrapping were used, as no yielding was anticipated here.

Post-tensioning was provided by a single 44.5-mm- (1-3/4 in.-) diameter, A722 Grade 150 steel threaded bar (Fig. 5a). The total effective post-tensioning force was 438 kN (98.5 kips) after losses. The bar ran within the column hollow core, and was screwed into an anchorage device prearranged in the footing, allowing for bar replacement. Additional deformability of the PT system was provided by placing a polyurethane pad in series with the PT bar, between the top anchorage plates and the load stub (Fig. 5b). Upon gap opening, the tensile deformation demand on the bar was partially converted into compressive deformation of the pad, preventing the bar from yielding and avoiding losses of PT and self-centering capacity. A disc consisting of 90-Shore-A hardness polyurethane, with a thickness of 47.6 mm (1-7/8 in.), a diameter of 190.5 mm (7.5 in.), and a central hole with a diameter of 57 mm (2-1/4 in.) was used for this scope. Its stiffness was 1.75×10^5 kN/m (1000 kip/in) when tested at ambient temperature and at a rate of 0.5 kips/sec.

(a) *(b)*

Fig. 4 – (a) Column base section, with visible metal ducts for dowels and bar heads. (b) Footing surface, with visible stainless-steel dowels and bar heads.

(a) *(b)*

Fig. 5 – (a) Column top section, with visible metal ducts for dowels, PT bar, and load-stub dowels during stub positioning. (b) PT bar top anchorage, with polyurethane pad (yellow).

4.2 Test Protocol

The column was subjected to three-dimensional shake-table excitation. The top block provided a translational mass of 2.4×10^4 kg (53 kips), a rotational inertia of 2.05 kg-m^2 (6.99×10^4 kip-in^2), and an axial load of 236 kN (53 kips).

A series of 8 ground-motion records from historical events was selected and scaled, based on the displacement demand imposed on a conventional reinforced-concrete column, designed according to California standards [1] and carrying the same mass block. The chosen records and the applied scale factors (SF) are summarized in Table 1. EQ1 was selected to maintain the column response within the elastic range. EQ2 and EQ3 represented frequent events with low ductility demands. EQ4 and EQ5 were chosen as design-level excitation. EQ6, EQ7, and EQ8 were intended to bring the conventional reinforced-concrete column to near-collapse conditions. EQ9 was a repeat of EQ5. Free-vibration tests were run at the beginning of the experiment, and white-noise tests were performed between the historical records to assess the dynamic properties of the system.

4.3 Test Results

Fig. 6a and Fig. 6b show the hysteretic overturning moment-drift ratio response in the two lateral directions. Lateral displacements at the center of mass have been normalized by the height of the center of mass above the column base, and thus, expressed as drift ratios; overturning moments have been normalized by the product of the block weight times the height of the center of mass above the column base. For drift ratios larger than 0.3%, it was observed that the base joint rotation was contributing to more than 90% of the lateral displacement: for this reason, drift ratios and joint rotations practically coincided. Fig. 7 illustrates the maximum and the residual drift ratio obtained during each run: recentering capacity was maintained throughout the test, with residual drift ratios always smaller than 0.6%.

At the end of EQ4 the mortar bed was flaking off without crushing. During EQ5 superficial crushing initiated on the north-east and south-west sides, and after EQ8 it extended all the way around the mortar bed (Fig. 8a). However, only the outermost 25-mm (1-in.) wide ring of mortar was damaged, while the inner portion was still sound. Some post-tensioning losses were recorded during the test, probably due to mortar plastic deformations preceding the full engagement of headed bars in transferring compression; at the end of the test they accounted for less than 30% of the initial force (after lock-off and creep losses). Negligible permanent deformations of the column concrete and of the steel shells were detected at the end of the test, when the specimen was lifted off the footing.

Table 1 – Selected ground-motion records and scale factors.

Test	Target Displ. Ductility Conv. Col.	Predicted Max Drift Ratio (%)	Event	Date	Station	SF
EQ1	<1.0	0.5	Coalinga	1983/05/09	Harris Ranch – Hdqtrs (temp)	2.50
EQ2	2.0	1.7	Imp. Valley	1979/10/15	EC Meloland Overpass FF	0.80
EQ3	2.0	2.5	Morgan Hill	1984/04/24	Coyote Lake Dam (SW abut)	0.70
EQ4	4.0	3.9	Northridge	1994/01/17	Rinaldi Receiving Station	0.56
EQ5	4.0	4.9	Northridge	1994/01/17	Sylmar – Olive View Med FF	-0.80
EQ6	8.0	8.2	Northridge	1994/01/17	Rinaldi Receiving Station	0.90
EQ7	8.0	8.3	Kobe	1995/01/16	Takatori	0.77
EQ8	10.0	8.8	Kobe	1995/01/16	Takatori	-0.90
EQ9	N.A.	N.A.	Northridge	1994/01/17	Sylmar – Olive View Med FF	-0.80

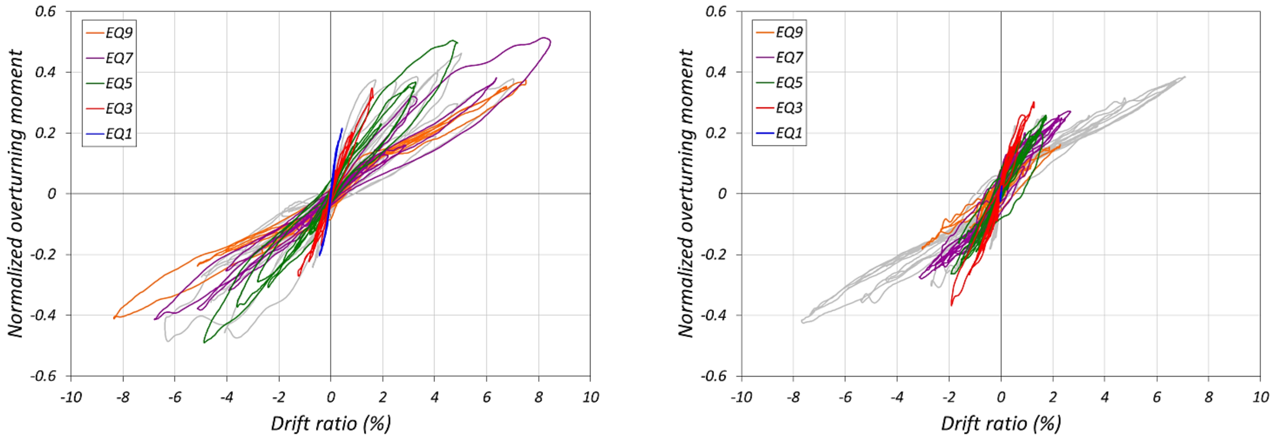

(a) (b)

Fig. 6 – Overturning moment-drift ratio response: (a) longitudinal direction; (b) transverse direction.

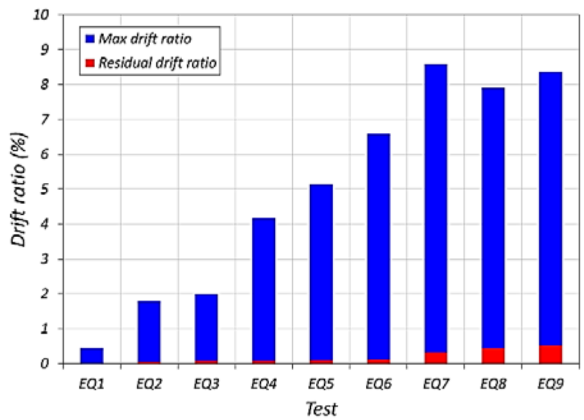

Fig. 7 – Maximum and residual drift ratios.

(a) (b)

Fig. 8 – Damage at the end of the test: (a) mortar bed superficial crushing; (b) stainless-steel dowel buckling and fracture.

Energy dissipators started fracturing under EQ6 test (6.6% maximum drift ratio), when one dowel fractured on the north-east side. Subsequently, three dowels were heard fracturing during EQ7 and other two during EQ8. After the test, when the column was separated from the footing, all dowels were found to have buckled and fractured (Fig. 8b).

4.4 Comparison with a Conventional Reinforced-Concrete Column

The experimental response of a conventional reinforced-concrete column conforming to California seismic standards [1], with the same dimensions and top mass as the dual-shell column, was investigated for comparative purposes [23]. The compressive strength of the conventional column concrete was 23 MPa (3.3 ksi) on the day of testing. Longitudinal reinforcement in the ratio of 1.6% was provided by 16 #4 (12.7-mm-diameter) bars, with yield stress from the 0.2% strain offset of 434 MPa (63 ksi), peak stress of 648 MPa (94 ksi), and peak strain of 12%. Transverse reinforcement was made of W4 spiral at 32-mm (1.25-in.) pitch, with yield stress from the 0.2% strain offset of 538 MPa (78 ksi), peak stress of 648 MPa (94 ksi), and peak strain of 1.1%; this provided a volumetric confinement ratio of 0.9%.

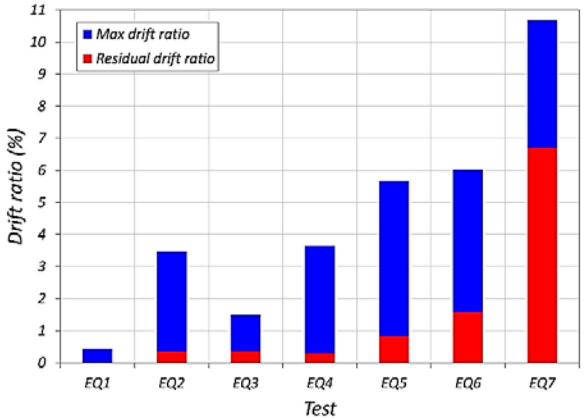

Fig. 9 – Maximum and residual drift ratios for the conventional reinforced-concrete column.

Fig. 10 – Damage at the end of the test of the conventional reinforced-concrete column.

Residual drift ratios on the order of 1% appeared since the end of EQ5 as shown in Fig. 9. Spalling of the concrete cover was observed during this same test. Transverse reinforcement did not fracture and preserved the vertical load carrying capacity of the concrete core, as intended by current design standards. Unexpectedly, longitudinal reinforcement did not buckle nor fracture at any time during the test: the narrow pitch of the spiral, at about 2.5 times the longitudinal bar diameter, might have caused this behavior. Damage conditions at the end of the test are shown in Fig. 10: extensive cover spalling was observed in the plastic-hinge region. The test was stopped after EQ7, as a peak drift ratio larger than 10% was reached and a residual drift ratio of nearly 7% was recorded. Note that the polarity of the vertical input motions for the conventional column was inverted, due to issues with the controller software; it is unclear if this had a significant effect on the overall performance of the structure.

5. Numerical Simulation of the Shake-Table Test

5.1 Modeling Approach

A three-dimensional numerical model of the test was developed and validated with the experimental results. For this purpose the software OpenSees [24][25] was used. More details can be found in Guerrini et al [19].

The column was modeled with two elastic beam-column elements in series, connected to the mortar bed at the base and to the loading point at the top; the intermediate node was used to connect the energy-dissipator elements. The stiffness of the lower segment was based on the concrete hollow section only, as the outer shell does not transfer directly compression at the interface (contact with the mortar is avoided), and tension is resisted by the energy dissipators at that location. Instead, the transformed-section stiffness was assigned to the upper segment, where the outer steel is effective in composite action with the concrete. The concrete elastic modulus was taken in accordance with design standards [1], based on its compressive strength on the day of testing. For the steel shells E_s = 200 GPA (29,000 ksi) was used. A node was defined at the center of mass of the top block to assign masses and vertical forces; since the deformations of the load stub and top block were expected to be negligible, this node was linked to the top of the column with a rigid element.

Multiple nonlinear truss elements [26][27][28] represented the mortar bed between column and footing; the mortar bed was discretized into 36 wedges along the circumference, and 3 rings along the radius. The length of the truss elements was set equal to the actual mortar thickness, i.e., 19 mm (0.75 in.). The *Concrete01* non-linear material model was assigned to these elements; this concrete-specific rule includes no tensile strength, which is appropriate for capturing gap opening. Peak stress and strain of 128 MPa (18.5 ksi) and 0.4%, respectively, were obtained from Mander's model for confined concrete [29], assuming a confinement efficiency coefficient equal to 0.1; this value was calibrated with the experimental results. The ultimate strain was set to 16%, with a residual stress of 6.9 MPa (1 ksi). Strains in the stress-strain relationship were amplified by the ratio of the theoretical neutral axis depth, calculated as 63.5 mm (2.5 in.), to the actual thickness of the mortar bed. With this transformation, the spread of inelastic behavior within the column concrete, assumed to extend uniformly for a length equal to the neutral axis depth [20], was approximately taken into account.

The post-tensioning bar was modeled as a nonlinear truss element, fixed at the base and connected to the top node of the column by a rigid element. An intermediate node was defined at the column-footing interface, to constrain lateral translation at that location. The *Steel02* material hysteretic rule [30], based on Giuffré-Menegotto-Pinto model, was assigned to it. An initial stress of 259 MPa (37.5 ksi) was set to represent the effective prestress after losses. An equivalent initial tangent elastic modulus and an equivalent bilinear factor were calculated, accounting for the stiffness of the urethane pad in series with the bar. The yield stress was set equal to 827 MPa (120 ksi). Curvature parameters R_0 = 18, c_{R1} = 0.925, and c_{R2} = 0.15 were chosen, while no isotropic hardening was introduced.

The energy-dissipating dowel bars were modeled as nonlinear displacement-based beam-column elements; the lower ends were fixed to the footing, while the upper ends were connected to the column intermediate node by rigid links. The element nonlinear properties were assigned in terms of internal forces rather than through fiber discretization, which is computationally burdensome; thus axial, flexural, and torsional behaviors were assigned to these elements at the cross-section level. The *Steel02* non-linear material model [30] was assigned to the dissipator axial and flexural relationships, while the torsional response was considered elastic. Three integration points were defined along each element, two at the ends and one in the middle: in fact, even though such elements are mainly subject to axial force, providing a minimum number of integration points would avoid numerical issues under bending. Geometry and material properties reflected the actual ones. However, the yield stress was set equal to 917 MPa (133 ksi) to better replicate the experimental monotonic stress-strain relationship of stainless-steel bars. Curvature parameters R_0 = 18, c_{R1} = 0.925, and c_{R2} = 0.15 were chosen, while no isotropic hardening was introduced.

The analysis was performed in two stages: first, the vertical load was applied and held constant; then the time-history analyses were run sequentially, keeping track of the cumulated residual deformations. The Newton-Raphson algorithm was chosen to solve the nonlinear residual equation, and the Newmark method was selected to integrate the equation of motion. Rayleigh damping was used: the contribution of the rigid links was excluded from the stiffness-proportional term, which was based on the initial stiffness; damping ratios of 1% were assigned to the first two modes (translational in the longitudinal and transverse directions). The analysis was performed under the hypothesis of large displacements, using the *co-rotational* geometric transformation in OpenSees.

5.2 Numerical Analysis Results

When analyzing the quasi-static cyclic tests of similar recentering dual-shell columns, modeled according to the same approach, Guerrini et al. [19] found good agreement between the numerical predictions and the experimental results, in terms of force-displacement relationship, cumulative energy dissipated, strain histories of the post-tensioning bars, and hysteretic axial stress-strain response of the energy dissipators, up to 5% drift ratios.

The numerical model was used to predict the maximum and residual drift ratios under the given set of ground motions, assigning the feedback records from the bare shake-table as inputs. Simulations were run up to EQ8, as the ninth run was added to observe the behavior of the damaged specimen under a design-level ground motion. Fig. 11 compares predicted and measured drift ratios. Good agreement can be observed between the maximum drift ratios, while relative discrepancy is found on the residual drift ratios when they are in the order of 0.1% or less (EQ1 to EQ6). However, since these quantities are very small, the resulting absolute error is negligible; moreover, residual drift ratios of 0.3% or larger (EQ7 and EQ8) are accurately predicted.

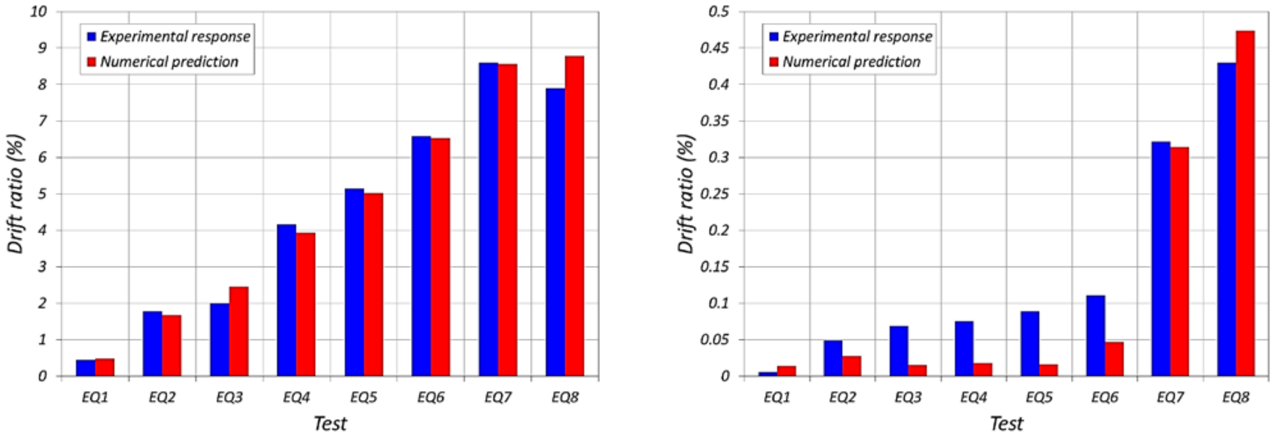

(a) *(b)*

Fig. 11 – Comparison between numerical prediction and experimental response: (a) maximum drift ratios; (b) residual drift ratios.

6. Conclusions

This paper discussed the experimental performance and numerical modeling of a composite concrete-dual steel shell bridge column technology. This column can be specifically designed for damage minimization at the design earthquake and to display a self-centering response. This technology, ideal for prefabrication, simplifies and accelerates bridge construction, as the outer shell makes the reinforcing cage obsolete, and the inner shell removes unnecessary concrete volume.

The use of a metallic-aggregate mortar bed incorporating polypropylene fibers, in combination with headed bars at the column-footing interface, delayed mortar crushing, and allowed the test unit to display excellent performance up to 8.6% drift ratio without losing recentering capacity. The polyurethane pad in series with the post-tensioning bar proved to be effective in preventing bar yielding, and consequent losses of prestress and of recentering behavior. Fracture of the energy dissipating dowels occurred at a drift ratio of 6.6%.

A comparison with a conventional reinforced concrete column response highlighted the main advantages of the proposed technology, in particular: (i) negligible residual drifts; (ii) minimal post-earthquake damage; (iii) reduction of repair costs; and (iv) mitigation of impacts on traffic, economy, and society.

The dynamic shake-table test was simulated in OpenSees environment, using a combination of truss and beam-column nonlinear elements. The numerical model accurately predicted the experimental response in terms of maximum and residual drift ratio demands, up to the final stages of testing.

7. Acknowledgements

Funding for this project, provided by the Pacific earthquake Engineering Research Center and by the California Department of Transportation, is gratefully acknowledged. The collaboration with Prof. Marc Eberhard, Prof. John Stanton, and Prof. Claudia Ostertag, and with Dr. Olafur Haraldsson, Dr. Marios Panagiotou, and Dr. William Trono is duly acknowledged. The contribution of Dr. Vesna Terzic is thankfully recognized. The assistance of the technical staff of the Charles Lee Powell Structural Engineering Laboratories at the University of California, San Diego, and of the PEER Center Laboratory at the University of California, Berkeley – Richmond Field Station, is gratefully recognized. The industry support by Hill Brothers Chemical Co., Salit Specialty Rebar, Headed Reinforcement Corp., and BASF-The Chemical Company is also thankfully acknowledged.

8. References

[1] Caltrans (2010). *Seismic Design Criteria*, California Dept. of Transportation, Sacramento, CA.

[2] AASHTO (2012). *AASHTO LRFD Bridge Design Specifications*, 6th Ed., American Association of State Highway and Transportation Officials, Washington, D.C.

[3] Palermo A., Pampanin S. (2008). Enhanced seismic performance of hybrid bridge systems: comparison with traditional monolithic solutions, *Journal of Earthquake Engineering*, **12**(8): 1267–1295.

[4] Mander J.B., Cheng C.-T. (1997). Seismic resistance of bridge piers based on damage avoidance Design, *Technical Report NCEER-97-0014*, NCEER, Department of Civil and Environmental Engineering, State University of New York at Buffalo, Buffalo, NY.

[5] Hewes J.T., Priestley M.J.N. (2002). Seismic design and performance of precast concrete segmental bridge columns, *Report No. SSRO-2001/25*, Department of Structural Engineering, University of California at San Diego, La Jolla, CA.

[6] Kwan W.P., Billington S. (2003). Unbonded posttensioned concrete bridge piers. I: monotonic and cyclic analyses, ASCE, *Journal of Bridge Engineering*, **8**(2): 92–101.

[7] Kwan W.P., Billington S. (2003). Unbonded posttensioned concrete bridge piers. II: Seismic analyses, ASCE, *J. Bridge Eng.*, **8**(2): 102–111.

[8] Sakai J., Mahin S.A. (2004). Analytical investigations of new methods for reducing residual displacements of reinforced concrete bridge column, *Report No. PEER 2004/02*, Pacific Earthquake Engineering Research Center, University of California, Berkeley, CA.

[9] Heiber D.G., Wacker J.M., Eberhard M.O., Stanton J.F. (2005). Precast concrete pier systems for rapid construction of bridges in seismic regions, *Report No. WA-RD 611.1*, Washington Department of Transportation, Olympia, WA.

[10] Palermo A., Pampanin S., Marriott D. (2007). Design, modeling, and experimental response of seismic resistant bridge piers with posttensioned dissipating connections, ASCE, *Journal of Structural Engineering*, **133**(11): 1648–1661.

[11] Marriott D., Pampanin S., Palermo A. (2009). Quasi-static and pseudo-dynamic testing of unbonded post-tensioned rocking bridge piers with external replaceable dissipaters, *Earthquake Engineering and Structural Dynamics*, **38**: 331–354.

[12] Solberg K., Mashiko N., Mander J.B., Dhakal R.P. (2009). Performance of a damage-protected highway bridge pier subjected to bidirectional earthquake attack, ASCE, *Journal of Structural Engineering*, **135**(5): 469–478.

[13] Ou Y.-C., Wang P.-H., Tsai M.-S., Chang K.-C., Lee G.C. (2010). Large-scale experimental study of precast segmental unbonded posttensioned concrete bridge columns for seismic regions, ASCE, *Journal of Structural Engineering*, **136**(3): 255–264.

[14] Culmo M.P. (2011). Accelerated bridge construction - experience in design, fabrication and erection of prefabricated bridge elements and systems, *FHWA Report HIF-12.013*, Federal Highway Administration Washington, D.C.

[15] FHWA (2012). http://www.fhwa.dot.gov/bridge/abc/index.cfm.

[16] Guerrini G., Restrepo J.I. (2011). Advanced precast concrete dual-shell steel columns, *Proceedings, 8th International Conference on Urban Earthquake Engineering*, **1**: 1125–1129, Tokyo, Japan.

[17] Restrepo J.I., Tobolski M.J., Matsumoto E.E. (2011). Development of a precast bent cap system for seismic regions, *NCHRP Report 681*, Transportation Research Board, Washington, D.C.

[18] Guerrini G., Restrepo J.I., Massari M., Vervelidis A. (2015). Seismic behavior of posttensioned self-centering precast concrete dual-shell steel columns, ASCE, *Journal of Structural Engineering*, **141**(4): 04014115.

[19] Guerrini G., Restrepo J.I., Vervelidis A., Massari M., (2015). Self-Centering Precast Concrete Dual-Steel-Shell Columns for Accelerated Bridge Construction: Seismic Performance, Analysis, and Design, *Report No. PEER 2015/13*, Pacific Earthquake Engineering Research Center, University of California, Berkeley, CA.

[20] Restrepo J.I., Rahman A. (2007). Seismic performance of self-centering structural walls incorporating energy dissipators, ASCE, *Journal of Structural Engineering*,**133**(11): 1560–1570.

[21] Gebman M., Ashford S., Restrepo J.I. (2006). Axial force transfer mechanisms within cast-in-steel-shell piles, *Report No. SSRP-94/10*, Department of Structural Engineering, University of California at San Diego, La Jolla, CA.

[22] Belleri A., Schoettler M.J., Restrepo J.I., Fleischman, R.B. (2013). Dynamic Behavior of Rocking and Hybrid Cantilever Walls in a Precast Concrete Building. ACI, *Structural Journal*, **111**(3): 661–672.

[23] Schoettler M., Eberhard M., Mahin S., Mosalam K., Ostertag C., Panagiotou M., Restrepo J., Stanton J., Terzic V. (2013). Advancing the performance of bridge columns: Overview of a shake table test program. *Proceedings, 7th National Seismic Conference on Bridges & Highways*, Paper No. 123, Oakland, CA.

[24] Mazzoni S., McKenna F., Scott M.H., Fenves G.L. et al. (2007). *OpenSees Command Language Manual*, Pacific Earthquake Engineering Research Center, University of California, Berkeley, CA.

[25] McKenna F., Scott M.H., Fenves G.L. (2010). Nonlinear finite element analysis software architecture using object composition, ASCE, *Journal of Computing in Civil Engineering*, **24**(1): 95–107.

[26] Taylor R.G. (1977). *The Nonlinear Seismic Response of Tall Shear Wall Structures*, Ph.D. Thesis, Department of Civil Engineering, University of Canterbury, Christchurch, New Zealand.

[27] Vulcano A., Bertero V.V. (1987). Analytical models for predicting the lateral response of RC shear walls: evaluation of their reliability, *Report No. UCB/EERC-87/19*, Earthquake Engineering Research Center, University of California, Berkeley, CA.

[28] Carr A.J. (2008). *Ruaumoko Manual*, Department of Civil Engineering, University of Canterbury, Christchurch, New Zealand.

[29] Mander J.B., Priestley M.J.N., Park R. (1988). Theoretical stress-strain model for confined concrete, ASCE, *Journal of Structural Engineering*, **114**(8): 1804–1826.

[30] Filippou F.C., Popov E.P., Bertero V.V. (1983). Effects of bond deterioration on hysteretic behavior of reinforced concrete joints, *Report No. UCB/EERC-83/19*, Earthquake Enigneering Research Center, University of California, Berkeley, CA.